Multi-rotor eVTOL Flight Simulation and Assessment under Atmospheric Turbulence

Matthew Bahr
Graduate Research Assistant

Ullhas Hebbar
Graduate Research Assistant

Etana Ferede
Research Scientist

Farhan Gandhi
Redfern Professor and MOVE Director

Center for Mobility with Vertical Lift
Rensselaer Polytechnic Institute
Troy, NY, United States

ABSTRACT

Atmospheric turbulence is applied to a 1200 lb quadcopter to evaluate the aircraft's rigid body response together with the rotor speed and motor current responses. Turbulence is generated using TurbSim to produce a full-field flow which is convected downstream over the aircraft. Three levels of turbulence intensity (mild, moderate, and severe) are applied to the aircraft, with the increasing levels of turbulence corresponding to higher velocity fluctuation in the flow-field. An outer loop flight controller, tuned to meet Level 1 handling qualities, is used to reject the disturbances to the aircraft airspeed. Various levels of turbulence produce larger aircraft response, with the severe case producing the largest peak-to-peak values for rigid body, rotor speed, and motor current response (4.74°, 114 RPM, and 160A, respectively). While the severe turbulence case is the most demanding on the motors, it is less than what has been previously seen for typical maneuvers. Therefore, motor size is limited by aircraft maneuver constraint, given the turbulence cases considered.

NOTATION

Symbols

i	Motor Current, A
I	Aircraft Inertia, kg m^2
V	Motor Voltage
V_x	Longitudinal Turbulent Velocity, m/s
V_y	Lateral Turbulent Velocity, m/s
V_z	Vertical Turbulent Velocity, m/s
θ	Aircraft Pitch Attitude, degrees
ϕ	Aircraft Roll Attitude, degrees
Ω	Rotor Speed, RPM
$\dot{\Omega}$	Instantaneous Change in Rotor Speed, rad/s^2

Acronyms

CFD	Computational Fluid Dynamics
eVTOL	Electric Vertical Takeoff and Landing
RMAC	Rensselaer Multicopter Analysis Code
TI	Turbulence Intensity
UAM	Urban Air Mobility
VTOL	Vertical Takeoff and Landing

Presented at the Vertical Flight Society's 77th Annual Forum & Technology Display, Virtual, May 10–14, 2021.

INTRODUCTION

Vertical lift aircraft have always provided a unique and indispensable ability to transport people and cargo in environments where traditional fixed wing aircraft cannot operate. The advent of distributed electric propulsion has simplified the operation of vertical takeoff and landing (VTOL) aircraft, creating the possibility for novel designs. Electric VTOL (eVTOL) aircraft with multiple lifting rotors is one example of popular aircraft designs in the Urban Air Mobility (UAM) market. Many manufacturers of varying backgrounds, such as the automaker Hyundai, the established VTOL manufacterer Bell, and the new eVTOL start-up Joby Aviation are developing aircraft to fill this market.

Aircraft designed for the UAM mission will operate in densely packed airspace within urban environments at relatively low altitudes (within the atmospheric boundary layer). Therefore, it is necessary to evaluate how various levels of turbulence will affect a representative multirotor eVTOL aircraft for UAM. In recent studies, the handling qualities of multirotor aircraft for UAM have been evaluated. Niemiec et al. (Ref. 1) used system identification methods to tune controllers based on handling qualities requirements for variable-pitch and variable-RPM quadcopters. Walter et al. (Ref. 2) evaluated the handling qualities of variable-RPM quadcopters of different sizes. A similar study by Bahr et al. (Ref. 3) focused on variable-RPM multicopters with four, six, and eight rotors. Both Refs. 2 and 3 determined the actuator requirements to follow certain maneuvers and reject discrete gusts. Similar work was done on larger aircraft in Refs. 4 and 5,

where the handling qualities of various multicopter configurations were used to evaluate the effectiveness of variable-RPM rotor control.

The disturbance rejection capabilities of small scale multicopters has also been evaluated in recent years. Disturbance rejection requirements were introduced during the control design process by Berrios et al. (Ref. 6) to improve the response of an identified aircraft in turbulent conditions. Similar identification methods were used by Lopez et al. (Ref. 7) to evaluate multicopters with different numbers of rotors in a gust wall of varying intensity. The authors found that overall a quadcopter had the best disturbance rejection capabilities, compared to a hexacopter and octocopter of similar weights.

In the past, research has been performed on conventional rotorcraft operating in turbulent conditions (Refs. 8–10). Those studies focused on the simulated response of a helicopter in discrete gusts and stochastic turbulence (Ref. 9), the affect that turbulence had on the handling qualities of the aircraft (Ref. 8), and the identification of a UH-60 response to turbulence and development of a low airspeed turbulence model (Ref. 10).

Further studies have focused on the operation of rotorcraft in ship airwakes. Thedin et al. (Ref. 11) applied steady and unsteady atmospheric boundary layer-based turbulent fields to evaluate the aircraft dynamics and vehicle response of an H-60 helicopter in the presence of a ship airwake. This study focused on the differences between the various modeling techniques for a single turbulence condition. Further, the pilot workload is evaluated by examining the frequency content of the pilot inputs, finding the most pilot workload occurs at low frequencies (0.1-1 Hz).

Another study involving a rotorcraft in a ship airwake introduced coupling of flight dynamics and CFD simulations (Ref. 12). This study focused on the vehicle response and control inputs for the aircraft in various flight conditions. While the simulations performed captured expected vehicle response and aerodynamic interactions, it came at the cost of large computation times (on the order of 3500 times slower than real time using 128 CPU cores).

The present study will apply CFD-based atmospheric turbulence to a 5340 N (1200 lb) quadcopter for UAM. Three different turbulence intensity cases are generated at various mean windspeeds. The applied turbulent flow-field will affect the forces and moments generated by each rotor, and impose drag-induced forces and moments on the aircraft rigid body. Flight simulations in the presence of turbulence are performed to evaluate the aircraft response to varying levels of atmospheric disturbances. Specifically, the rigid body response and rotor speed response will be examined. Ultimately, the actuator effort (the motor current and torque) required to reject the disturbances will be identified.

AIRCRAFT MODEL

The aircraft modeled in this study is an edge-first fixed pitch, variable-RPM quadcopter (the same quadcopter from Ref. 3), shown in Fig. 1. The aircraft has a gross weight of 5340 N (1200 lb) and the boom lengths are sized to maintain a 10% rotor tip-to-tip clearance. The aircraft parameters are shown in Table 1. Due to the symmetry of the vehicle, $I_{xy} = I_{xz} = I_{yz} = 0$.

Table 1: Quadcopter Parameters

Parameter	SI	Customary
Gross Weight	5340 N	1200 lb
Disk Loading	287 N/m^2	6 psf
Rotor Radius	1.22 m	4 ft
Total Disk Area	18.6 m^2	200 ft^2
Boom Length	1.81 m	5.94 ft
I_{xx}	344 kg m^2	466 slug ft^2
I_{yy}	405 kg m^2	549 slug ft^2
I_{zz}	667 kg m^2	904 slug ft^2
Rotor Root Pitch	21.5°	
Rotor Twist	-10.4°	
Tip Clearance	0.1R	

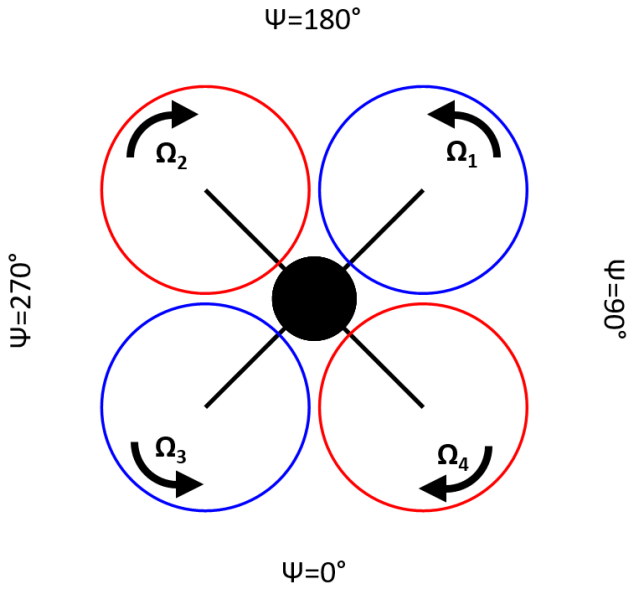

Figure 1: Quadcopter

The flight dynamics are modeled using the Rensselaer Multicopter Analysis Code (RMAC, Ref. 13), which calculates the aircraft accelerations by summation of forces and moments at the aircraft center of gravity. The forces and moments produced by each rotor are calculated using blade element theory and a 3x4 Peters-He finite-state dynamic wake model (Ref. 14). RMAC is used to trim the aircraft, generate linear models for flight control design, and evaluate the nonlinear dynamics during flight simulations.

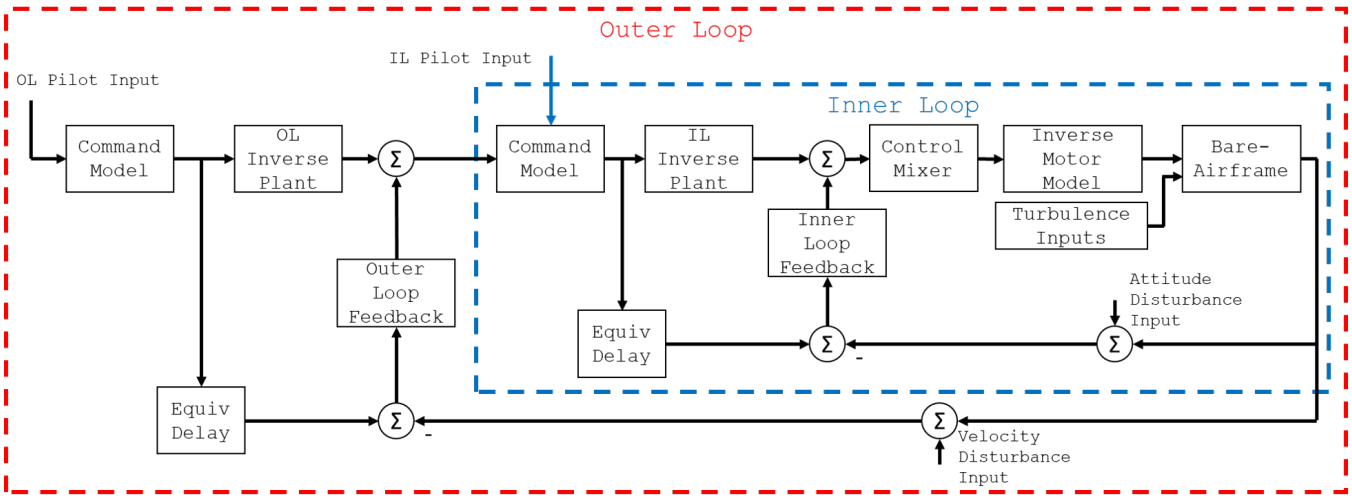

Figure 2: Control Architecture

Control Architecture

The controller used in this study is the same as the quadcopter controller used in Ref. 3, and is shown in Fig. 2. It is an explicit model following controller which features PID feedback controllers with feedforward paths using an inverse model. The inverse model parameters used in the feedforward paths are defined about the aircraft in hover.

The control optimization tool CONDUIT® (Ref. 15) is used to tune the flight controller to meet stability, handling qualities, and performance requirements. Included in the handling qualities requirements are disturbance rejection specifications, which are given by ADS-33E-PRF (Ref. 16). In this study, an outer loop controller is implemented, which will reject disturbances to the aircraft groundspeed. The controller gains used are identical to what was used in Ref. 3, and more detail regarding the flight controller and the control optimization results can be found in Ref. 3.

TURBULENT VELOCITY GENERATION

Generation of a realistic turbulent flow-field is paramount to ensuring an accurate flight dynamics simulation. Several methods can be employed to this end: a) A time series of uncorrelated velocity vectors specified at every desired node of interest drawn from an appropriate frequency spectrum (Kaimal, von Karman etc.); b) Using a precursor CFD simulation which generates the turbulent flow-field by applying a suitable pressure gradient and well-chosen initial and boundary conditions; c) Imposing resolved turbulence (from a wind-field generator) at the inlet of a CFD simulation and convecting the data downstream to the region of interest. The third method is employed in this work with TurbSim (developed by NREL, Ref. 17) as the stochastic turbulence generation code producing a full-field flow that includes bursts of coherent turbulence with spatiotemporal consistency related to turbulent structures (eddies) in the flow. This method ensures realistic large-scale coherent structures in the wind-field while avoiding an expensive precursor simulation.

The two-dimensional fluctuating wind profiles from the stochastic generator are prescribed as an inlet boundary condition (BC) to the finite-element based CFD solver PHASTA which simulates the convection of the TurbSim specified inlet flow-field over the quadcopter. The 2D velocity profile at the inlet was generated over a 15 m $\times$ 15 m square patch using a grid-spacing of 0.25 m, resulting in 61 nodes on each side of the square. In order to smoothly transition from the turbulent patch to the non-turbulent free-stream flow outside the patch, a 10 point (or 2.5 m) buffer zone was utilized on all sides and equipped with a linear weighting function such that fluctuations go to zero at the outer edges of the square patch (Ref. 18). The TurbSim data generation used a time step of 0.1 seconds and a linear temporal interpolation kernel then was used to generate data at the finer CFD time step of 0.05 seconds at the inlet face. The inlet turbulence was convected downstream using a structured grid with a 0.5 m grid spacing in all directions and a cuboidal slice of dimensions 10 m $\times$ 10 m $\times$ 1.5 m comprising two minutes of fluctuating nodal velocities was extracted for the flight dynamics routine. The cuboidal slice was chosen to ensure full coverage of the quadcopter's operating extents at a pitch attitude of up to 12°.

Figure 3 shows an example of instantaneous resolved turbulence washing over the quadcopter. The solid black arrow represents the direction of flow field convection. Each vertical slice represents the magnitude of the edgewise turbulent velocity (along the direction of the black arrow). At time t features of high windspeed (dark red color) are seen on the top portion of the flow field in the middle slices. After some duration of time (Δt) the high windspeed features have convected downsteam to the top of the right most vertical slices of the flow field while the low-speed features are convected more slowly. This physically represents the content of the turbulent flow field moving from the front rotors (rotors 1 and 2) to the rear rotors (rotors 3 and 4) after some Δt.

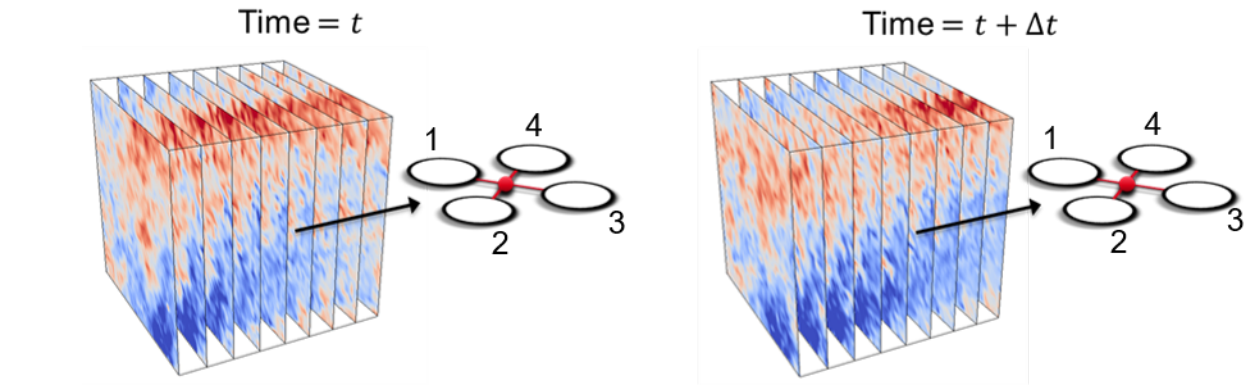

Figure 3: Instantaneous Vertical Slices of Turbulent Edgewise Velocity Field (Quadcopter Shown Outside Flow-Field for Visual Clarity)

TURBULENCE IMPLEMENTATION

Three cases of turbulence intensity are considered in this study: a mild, moderate, and severe case, which are summarized in Table 2. The mean windspeed represents the mean wind velocity in the direction of flight.

Table 2: Turbulent Cases

	Mild	Moderate	Severe
Turbulence Intensity	15%	30%	30%
Mean Windspeed	5.14 m/s (10 kt)	5.14 m/s (10 kt)	10.3 m/s (20 kt)

The aircraft trim solution is found given the mean airspeed of the turbulent field for the different turbulence cases, the different trim solutions are shown in Table 3. Due to the geometry of the aircraft, the four rotors always share a plane. Using this, a single plane is interpolated from the cuboidal grid generated by the CFD solver at the trim pitch attitude.

Table 3: Aircraft Trim

Trim Parameter	Value	
Airspeed	5.14 m/s (10 kt)	10.3 m/s (20 kt)
θ	-0.79°	-1.64°
$\Omega_{1,2}$	1040 RPM	980 RPM
$\Omega_{3,4}$	1105 RPM	1095 RPM
$V_{1,2}$	135 V	127 V
$V_{3,4}$	144 V	142 V
$i_{1,2}$	135 A	117 A
$i_{3,4}$	154 A	148 A

The turbulent velocities are interpolated at five regions within the plane, the four rotor hubs and the aircraft center of gravity. The velocities applied to the center of gravity are used to calculate the drag on the aircraft due to turbulence. For each individual rotor the velocities at the hub are used to calculate how the inflow evolves over time. Most importantly, the turbulent velocity is interpolated and applied over the rotor disk (40 points along the blade, and 96 points about the rotor azimuth, totalling 3840 points) to calculate the inflow and forces and moments generated (using blade element theory) for each rotor.

The aircraft is assumed to be spatially fixed in the turbulent field, with the flow field convecting over the aircraft at the mean windspeed. Use of an outer loop controller will ensure the aircraft maintains zero groundspeed while experiencing a turbulent headwind. While a position hold controller is not present in this study, the outer loop controller will command the aircraft to hover. It is also assumed that the attitude deviations of the aircraft will be small, therefore the turbulent plane is fixed and does not rotate with the aircraft (the plane is interpolated once).

The time histories for the turbulent velocities at the hubs of rotors 1 and 4 are shown in Figs. 4-9 for the various levels of turbulence intensity and mean windspeed. Dashed black vertical lines are drawn on the rotor 1 time histories at instances where there is a notable feature in the longitudinal turbulent velocity, V_x. The vertical line is drawn at the same time on the rotor 4 plot, for the same turbulence case. This shows that rotor 4 sees similar turbulence content as rotor 1. For example, Fig. 4 shows a sharp increase in V_x at $t = 46.7s$ for rotor 1. Figure 5 shows that the same sharp increase seen by rotor 1 occurs a fraction of a second later on rotor 4. This delay is caused by the time it takes for the turbulent field to convect downstream. Similar behaviour can be seen for each turbulence case, rotor 4 sees a similar turbulent velocity profile as rotor 1. However, since the flow field both convects downstream and evolves over time, rotor 4 never sees the same exact velocities as rotor 1.

The frequency content in each axis for the three levels of turbulence is shown in Figs. 10-12. The longitudinal turbulent velocity (Fig. 10) has the most frequency content out of all the axes. Referring back to the time domain plots (Figs. 4-9) shows that in all cases the longitudinal axis has both the highest mean velocity and most variations in windspeed.

In all axes the vertical shift (increased gain) in the frequency response is caused by the increased magnitude of the eddies present in the turbulent field. Moving from the Mild

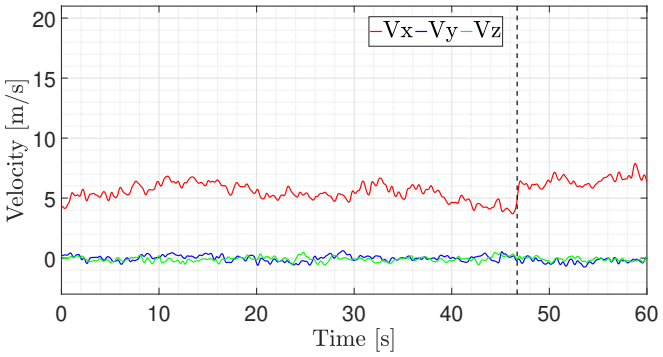

Figure 4: Rotor 1 Hub Velocities Mild Turbulence

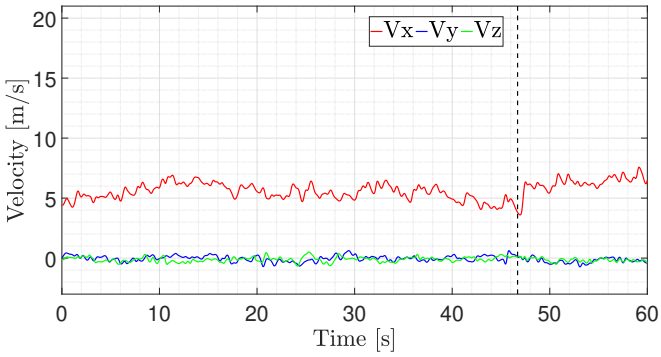

Figure 5: Rotor 4 Hub Velocities Mild Turbulence

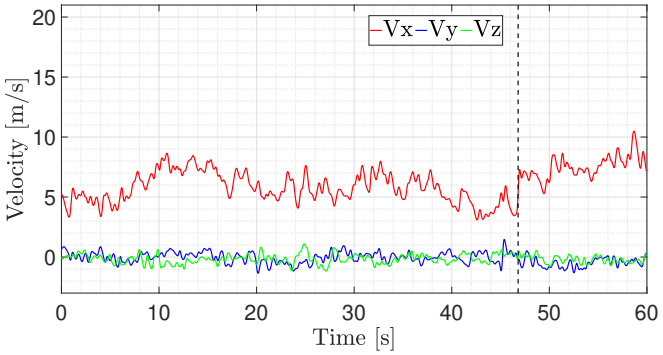

Figure 6: Rotor 1 Hub Velocities Moderate Turbulence

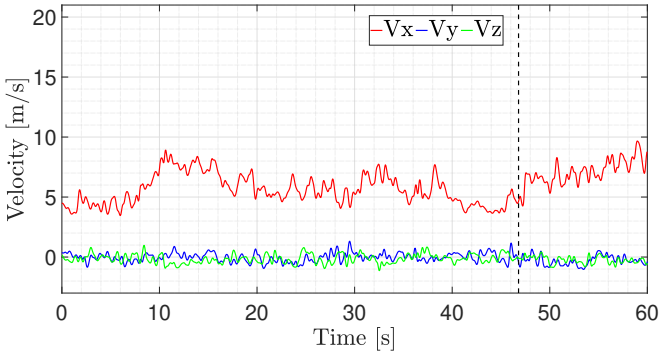

Figure 7: Rotor 4 Hub Velocities Moderate Turbulence

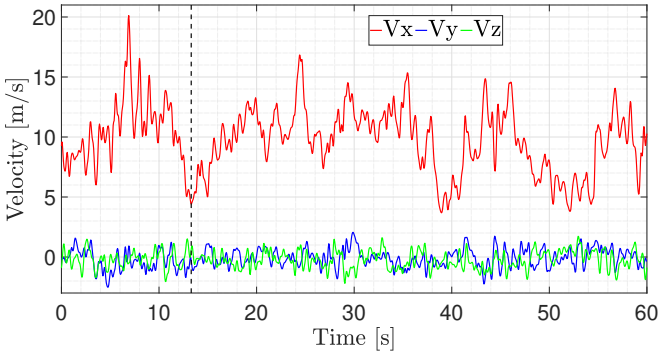

Figure 8: Rotor 1 Hub Velocities Severe Turbulence

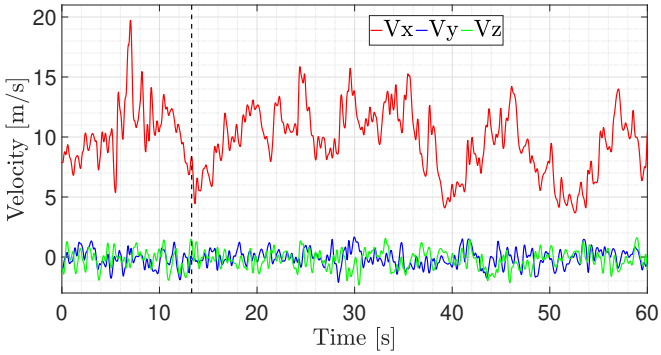

Figure 9: Rotor 4 Hub Velocities Severe Turbulence

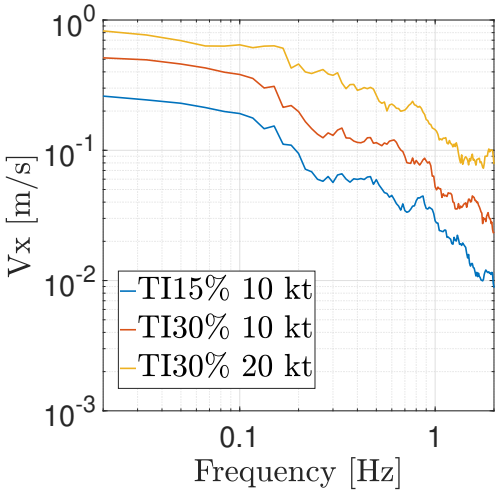

Figure 10: Rotor 1 Hub Longitudinal Turbulent Velocities Frequency Content

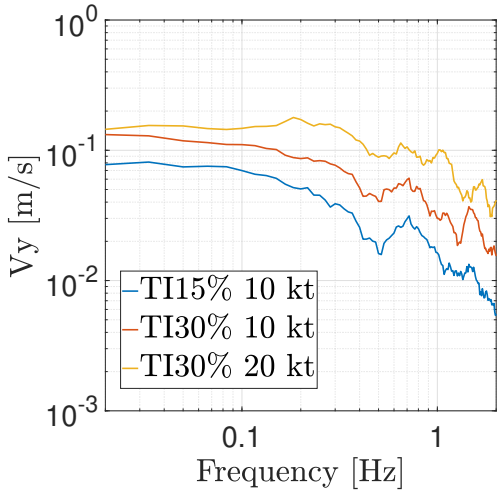

Figure 11: Rotor 1 Hub Lateral Turbulent Velocities Frequency Content

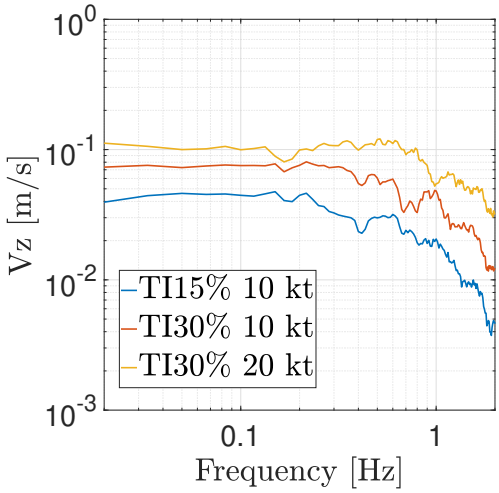

Figure 12: Rotor 1 Hub Axial Turbulent Velocities Frequency Content

to Moderate turbulence cases (Table 2) increases the magnitude of the eddies due to the increase in turbulence intensity (15%TI $\rightarrow$ 30%TI). The Moderate to Severe cases have the same turbulence intensity level (Table 2), but the mean windspeed doubles (10 knots $\rightarrow$ 20 knots) which will also increase the magnitude of the eddies. The corner frequency of the axial turbulent velocity (Fig. 12) also changes with the mean windspeed. For the Mild and Moderate cases the corner frequency is about 0.2 Hz, but the Severe case has a corner frequency of about 0.6 Hz. The increase in windspeed causes the eddies in the induced velocity field to move faster over the aircraft, which shifts the frequency content.

RESULTS

Three different turbulence cases are applied to evaluate the rigid body, rotor speed, and motor current response of the aircraft. The rigid body response (the change in attitude) shows the effect the turbulence has on the aircraft as a whole. In order to reject the disturbances caused by turbulence the rotors will need to constantly change speed (due to fixed pitch rotors). These rapid changes in rotor speed create current demands that the motors must be capable of meeting.

The attitude response to turbulence is shown in Figs. 13-15. The primary response is in the roll and pitch axes, with no observable deviation in yaw occurring. The pitch axis sees the largest disturbance in all turbulence cases, which is due to the longitudinal axis having the highest turbulence (Fig. 10). The peak-to-peak pitch response for all cases is tabulated in Table 4.

Table 4: Peak-to-Peak Pitch Response

Turbulence Case	Peak-to-Peak Pitch
Mild	1.41°
Moderate	3.83°
Severe	4.74°

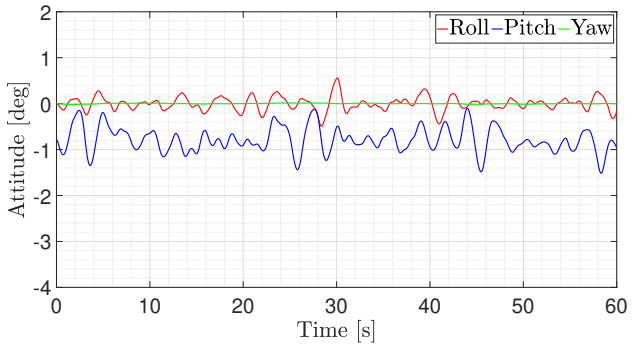

Figure 13: Mild Turbulence Attitude Response

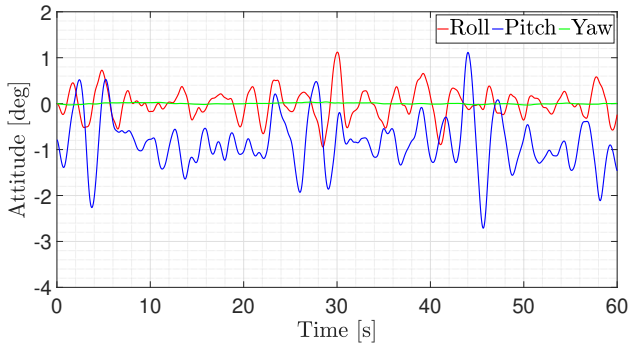

Figure 14: Moderate Turbulence Attitude Response

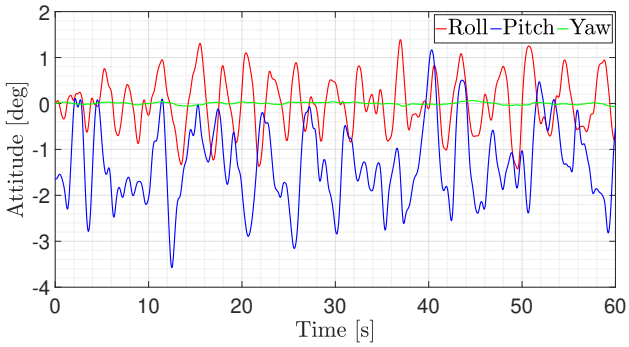

Figure 15: Severe Turbulence Attitude Response

As the turbulence increases in intensity (from mild to moderate to severe) the attitude disturbances increase in magnitude. The more intense turbulence cases have larger variations in wind velocities in all axes. This will affect the rigid body response in by varying the inflow at each rotor, therefore changing the forces and moments produced.

The rotor speed for rotor 4 in the different turbulence conditions is shown in Fig. 16. The rotor speeds for rotor 4 are directly compared because the trim rotor speed at the two windspeeds is similar (Table 3). The mild turbulence case has the smallest deviations in speed, while the moderate turbulence case causes an increase in rotor speed activity. However, the severe case causes significantly larger changes in rotor speed. As previously discussed, the various levels of turbulence intensity will increase and decrease the forces and moments produced by the rotors, causing deviations from desired the airspeed.

When the turbulence becomes more severe the rotors are required to be more active to reject the increasing level of disturbances. This additional activity is seen in the increase in the peak-to-peak rotor speed values, which are tabulated in Table 5. The increase in the peak-to-peak rotor speeds will demand the rotors change speed quicker. This variation in $\dot{\Omega}$ (the instantaneous change in rotor speed) will create surges in current that the drivetrain must be capable of providing.

The frequency content of absolute motor 1 current for the different turbulence cases is shown in Fig. 17. At low frequencies (0.1-0.4 Hz) the current magnitude is strongly influenced by the turbulence intensity. In this frequency range the two TI 30% cases are similar, seen as the red and yellow curves

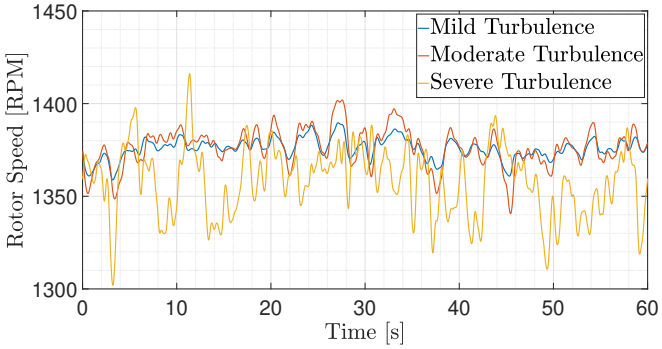

Figure 16: Rotor 4 Speed Response to Various Turbulence Cases

Table 5: Peak-to-Peak Rotor Speed Values

Turbulence Case	Peak-to-Peak Rotor Speed [RPM]
Mild	30.8
Moderate	61.3
Severe	114

being close together. Both the 10 knot windspeed cases have a corner frequency of about 0.4 Hz. However, the 20 kt case has a corner frequency of about 1 Hz. The frequency response of motor 1 current closely resembles the frequency content of the axial turbulence (Fig. 12). Variations in axial flow through a rotor significantly effect the thrust produced. This deviation from nominal thrust will cause disturbances in the rigid body response of the aircraft, which the flight controller will compensate for.

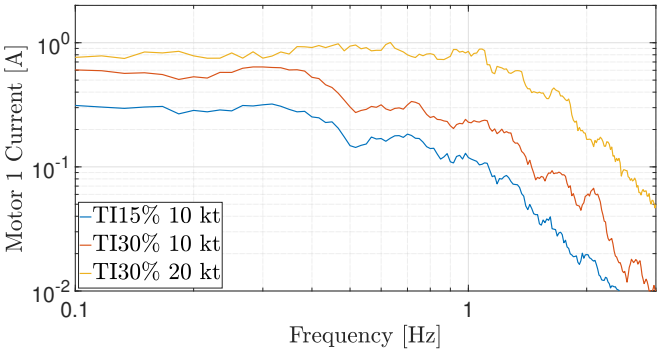

Figure 17: Motor 1 Current Frequency Content

The peak current and torque values for the turbulence cases are tabulated in Table 6. Continuing the trend seen by the rigid body and rotor speed responses, the motor current requirements increase with turbulence intensity. The peak current requirement is an important value for motor sizing and aircraft design, as the current is correlated to the weight via torque (Ref. 19). In order to avoid actuator saturation in the presence of turbulence, the individual motors must be sized to meet the peak current requirements. This however comes at the cost of increased motor mass, decreasing the payload, flight time, or range capabilities. The peak torque is calculated by $Q = i * K_t$, where i is the peak current, and K_t is the motor torque constant (equivalent to back-EMF constant if using SI units). The motors assumed for the quadcopter in this study have a torque constant of $K_t = 1.18$ Nm/A (Ref. 3).

Table 6: Peak Motor Current and Torque Values

Turbulence Case	Peak Current [A]	Peak Torque [Nm]
Mild	160	189
Moderate	167	197
Severe	172	203

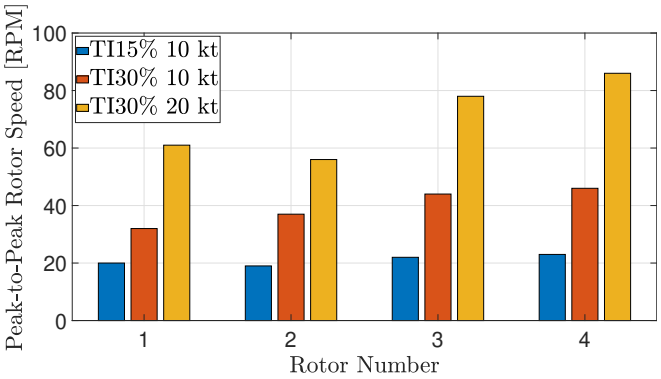

Figure 18: Peak-to-Peak Rotor Speeds

In all turbulence cases, the rear rotors experience the peak current, and therefore torque. Normalizing by the trim current for rotor 3 gives the margin required to reject the disturbances. The mild case requires a current margin of 3.9%, moderate requires 8.4%, and the severe case requires the most at 16.2%. These current requirements are much lower than the what was required for maneuvers from Ref. 3, where the lowest current margin required was 33% for a 10° pitch doublet.

The peak-to-peak values for rotor speed, motor voltage, and motor current for all rotors are summarized in Figs. 18-20. In all cases the increase in turbulence intensity increases the peak-to-peak values for each rotor. Overall, the rear rotors (rotors 3 and 4) see the largest peak-to-peak values.

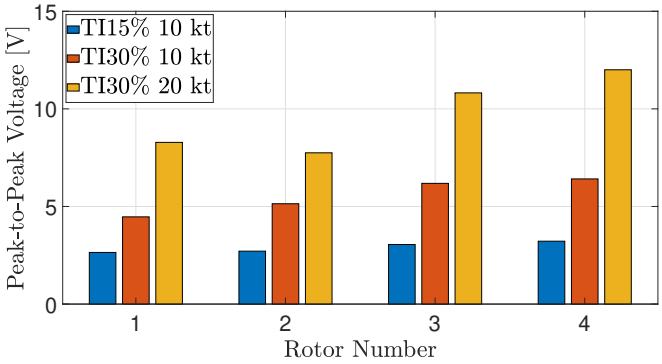

Figure 19: Peak-to-Peak Motor Voltage

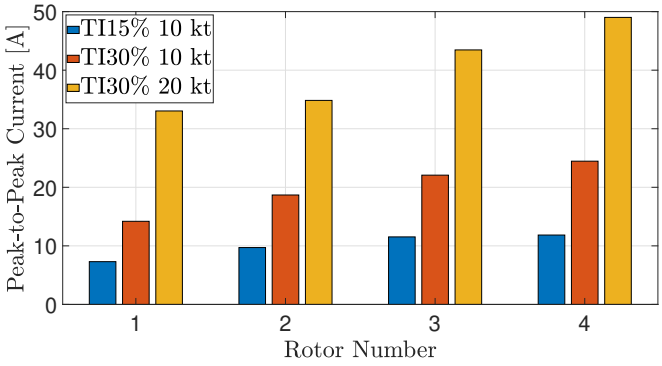

Figure 20: Peak-to-Peak Motor Current

CONCLUSIONS

This study applied CFD-based atmospheric turbulence to a 5340 N (1200 lb) quadcopter aircraft for UAM. Three levels of turbulence intensity are generated and applied to the spatially fixed aircraft. The flow field evolves over time and convects over the aircraft, affecting the forces and moments produced by the rotors, and the drag on the aircraft. Flight simulations were performed on the aircraft using an outer loop controller to maintain desired airspeed.

Higher levels of turbulence results in larger variation in aircraft response. The peak-to-peak values of aircraft attitudes, rotor speeds, motor voltage, and motor current (and torque) increase with turbulence intensity. Under severe turbulence, 4.7° peak-to-peak change in pitch is observed. To reject this severe atmosphere disturbance, the rotors see a peak-to-peak change of 114 RPM. The necessary motor torque to change the speed of the rotors is 203 Nm. This corresponds to a peak current of 172A, or 16% more than the trim current.

Overall, the quadcopter and flight controller were able to reject the disturbances for all turbulence cases considered without excessive actuator requirements. Moving forward, more extreme turbulence cases can be evaluated on the aircraft. Another potential avenue is redesigning the flight controller to improve the disturbance rejection capabilities. Furthermore, a position hold controller can be implemented to better represent actual usage cases.

Author contact:

Matthew Bahr:	bahrm2@rpi.edu
Etana Ferede:	ferede@rpi.edu
Ullhas Hebbar:	udayau@rpi.edu
Farhan Gandhi:	gandhf@rpi.edu

ACKNOWLEDGMENTS

This work is carried out at Rensselaer Polytechnic Institute under the Army/Navy/NASA Vertical Lift Research Center of Excellence (VLRCOE) Program, grant number W911W61120012, with Dr. Mahendra Bhagwat as Technical Monitor.

REFERENCES

1. Niemiec, R., Gandhi, F., Lopez, M. J. S., and Tischler, M. B., "System Identification and Handling Qualities Predictions of an eVTOL Urban Air Mobility Aircraft Using Modern Flight Control Methods," Vertical Flight Society 76th Annual Forum, Virtual, October 6–8, 2020.

2. Walter, A., McKay, M., Niemiec, R., and Gandhi, F., "Hover Handling Qualities of Fixed-Pitch, Variable-RPM Quadcopters with Increasing Rotor Diameter," Vertical Flight Society 76th Annual Forum, Virtual, October 6–8, 2020.

3. Bahr, M., McKay, M., Niemiec, R., and Gandhi, F., "Handling Qualities Assessment of Large Variable-RPM Multi-Rotor Aircraft for Urban Air Mobility," Vertical Flight Society 76th Annual Forum, Virtual, October 6–8, 2020.

4. Malpica, C., and Withrow-Maser, S., "Handling Qualities Analysis of Blade Pitch and Rotor Speed Controlled eVTOL Quadrotor Concepts for Urban Air Mobility," VFS Inernational Powered Lift Conference 2020, San Jose, CA, January 21–23, 2020.

5. Withrow-Maser, S., Malpica, C., and Nagami, K., "Multirotor Configuration Trades Informed by Handling Qualities for Urban Air Mobility Application," Vertical Flight Society 76th Annual Forum & Technology Display, Virtual, October 6–8, 2020.

6. Berrios, M. G., Berger, T., Tischler, M. B., Juhasz, O., and Sanders, F. C., "Hover Flight Control Design for UAS Using Performance-based Disturbance Rejection Requirements," AHS 73rd Annual Forum, Fort Worth, TX, May 9–11, 2017.

7. Lopez, M. J. S., Tischler, M. B., Juhasz, O., Gong, A., Sanders, F. C., Soong, J. Y., and Nadell, S. J., "Flight Test Comparison of Gust Rejection Capability for Various Multirotor Configurations," Vertical Flight Society 75th Annual Forum & Technology Display, Philadelphia, PA, May 13–16, 2019.

8. Hess, R., "Rotorcraft Handling Qualities in Turbulence," *Journal of Guidance, Control, and Dynamics*, Vol. 18, (1), 1995, pp. 39–45. DOI: 10.2514/3.56654

9. Dahl, H., and Faulkner, A., "Helicopter Simulation in Atmospheric Turbulence," Fourth European Rotorcraft and Powered Lift Aircraft Forum, Munich, Germany, September 13–15, 1978.

10. Lusardi, J. A., Tischler, M. B., Blanken, C. L., and Labows, S. J., "Empirically Derived Helicopter Response Model and Control System Requirements for Flight in Turbulence," *Journal of the American Helicopter Society*, Vol. 49, (3), 2004, pp. 340–349. DOI: 10.4050/JAHS.49.340

11. Thedin, R., Murman, S. M., Horn, J., and Schmitz, S., "Effects of Atmospheric Turbulence Unsteadiness on Ship Airwakes and Helicopter Dynamics," *Journal of Aircraft*, Vol. 57, (3), 2020, pp. 534–546. DOI: 10.2514/1.C035643

12. Oruc, I., Horn, J. F., Polsky, S., Shipman, J., and Erwin, J., "Coupled Flight Dynamics and CFD Simulations of the Helicopter / Ship Dynamic Interface," American Helicopter Society 71st Annual Forum, Virginia Beach, VA, May 2015.

13. Niemiec, R., and Gandhi, F., "Development and Validation of the Rensselaer Multicopter Analysis Code (RMAC): A Physics-Based Comprehensive Modeling Tool," Vertical Flight Society 75th Annual Forum, Philadelphia, PA, May 12–16, 2019.

14. Peters, D., Boyd, D., and He, C. J., "Finite-State Induced-Flow Model for Rotors in Hover and Forward Flight," *Journal of the American Helicopter Society*, Vol. 34, (4), 1989, pp. 5–17.

15. Tischler, M., Berger, T., Ivler, C., Mohammadreza, M. H., Cheung, K. K., and Soong, J. Y., "Practical Methods for Aircraft and Rotorcraft Flight Control Design: An Optimization-Based Approach," AIAA Education Series, Reston, VA, 2017.

16. "Aeronautical Design Standard, Performance Specification, Handling Qualities Requirements for Military Rotorcraft," Technical Report ADS-33E-PRF, March 2000.

17. Kelley, N., and Jonkman, B., "Overview of the TurbSim Stochastic Inflow Turbulence Simulator," Technical Report National Renewable Energy Lab (NREL), Golden, CO, 2006.

18. Hebbar, U., Rane, J., Gandhi, F., and Sahni, O., "Analysis of Interactional Aerodynamics in Multi-Rotor Wind Turbines using Large Eddy Simulations," AIAA SciTech Forum, Orlando, FL, January 6–10, 2020.

19. Johnson, W., "NDARC - NASA Design and Analysis of Rotorcraft," Technical Report NASA TP 218751, April 2015.